ANALYZING THE IMPACT OF LOW-TO-MODERATE EARTHQUAKE IN KON TUM, VIETNAM BY TIME-SERIES SENTINEL-1A

Le Minh Hang[1], Tran Van Anh[2], Do Thi Hoai[3]
[1]Le Quy Don Technical University, 236 Hoang Quoc Viet Street, Bac Tu Liem, Hanoi, Vietnam,
Email: leminhhang81@lqdtu.edu.vn
[2]Hanoi University of Mining and Geology, No.18 Vien Street, Duc Thang Ward, Bac Tu Liem, Hanoi, Vietnam,
Email: tranvananh@humg.edu.vn
[3]Vietnam Institute of Geodesy and Cartography, 479 Hoang Quoc Viet Street, Bac Tu Liem District, Hanoi, Vietnam
Email: hoaivo1976@gmail.com

KEY WORDS: low-to-moderate earthquake, time-series Sentinel-1A, PSInSAR method.

ABSTRACT: In 2021 and 2022, the province of Kon Tum in Vietnam had a number of low-to-moderate earthquakes with magnitudes between 2.5 and 4.8 on the Richter scale. The primary causes of these earthquakes are geological activity and hydroelectric development projects in the area. The DInSAR technique is primary tool for monitoring the earthquakes, volcano. Sentinel-1 satellite images, which are openly accessible for a period of 12 days, are currently the main source of data for monitoring surface displacement. In this work, we use time-series Sentinel-1A images and Persistent Scatterer Interferometry (PSInSAR) techniques to analyze and assess the effects of low to moderate earthquakes in Kon Tum. The Sentinel-1A images were used from April 2021 to July 2022. According to the data, the Kon Tum area had a mean displacement velocity of -21.3 mm to 20.3 mm per year between 2021 and 2022. There has been an abnormal displacement and subsidence of approximately 40 mm, particularly in the area that is near the epicenter location.

1. INTRODUCTION

More than 100 earthquakes with magnitudes smaller than 4.0 on the Richter scale occurred between April 2021 and July 2022, with their epicenters in the Kon Plong district, Kon Tum province, Vietnam. In particular, an earthquake of a moderate magnitude of 4.8 on the Richter scale occurred in the Kon Plong area on April 18, 2022, and the hypocentral depth was 8.1 km. The cause of the earthquake was due to the influence of the hydroelectric reservoirs' water storage activities in the area. Low-to-moderate earthquakes at Kon Tum did not harm people or property, but they did prove the area's unstable ground. The Rao Quang-A Luoi fault line, which runs through Kon Plong district, Kon Tum province, Vietnam, is where the earthquake-prone regions are.

Synthetic Aperture RADAR (SAR) is an active microwave remote sensing system that can operate in all weather conditions and is not affected by haze from clouds. Sentinel-1A satellite has a microwave sensors, band C and 12-day orbit cycles. Additionally, control in a narrow tube will aid in reducing the spatial baseline in interferometry processing. This particular design provides a quick response with InSAR to earthquakes and supports the production of interferograms with high interferometry coherence, particularly in low-latitude regions with thick plant cover.

The InSAR method has been shown to be effective for observing earthquakes (Biggs and Wright, 2020; Bignami, et al., 2021; Eyidogan and Barka, 1995; Furuya and Satyabala, 2008; Ghayournajarkar and Fukushima, 2020), as well as volcanoes (Catry, et al., 2015; Gatsios, et al., 2020). Many studies show that the InSAR method accurately determines surface displacement and provides more accurate information about earthquake effects than traditional measurement methods (Ghayournajarka and Fukushima, 2020; Gong, et al., 2011). Radarsat (Elske, et al., 2012), EnviSAT ASAR (Furuya and Satyabala, 2008; Moro, et al., 2017), ALOS PALSAR (Ghayournajarkar and Fukushima, 2022; Huang, et al., 2014; Liu, et al., 2022), and Sentinel-1A and Sentinel-1B (Bignami, et al., 2021; Ghayournajarkar and Fukushima, 2020; Li, et al., 2021a; Li, et al., 2021b) are the SAR images used in earthquake research by the InSAR method. Research results have proved that Sentinel-1 data is suitable for monitoring the deformation of terrain after earthquakes globally (Li, et al., 2021a). (Tong, et al., 2022) determined the coseismic slip model of an earthquake Mw 7.3 in Maduo Country, Qinghai Province, China, using Sentinel-1 imagery and the InSAR method. The length of the surface rupture is more than 140km as determined by the InSAR technique, and the LOS (line-of-sight) displacement is approximately 2m. (Zhao, et al., 2021) used 45 Sentinel-1 images to detect and analyze ground displacement caused by small magnitude earthquakes in Rong Country, China using the D-InSAR technique combined with GACOS atmospheric correction. The research results show that the atmospheric correction by the GACOS method helps to increase the accuracy of determining seismic displacement. Studies show that earthquakes Mw $\geq$ 5 will cause a displacement of several centimeters and are easily detected by D-InSAR. Earthquakes Mw<5 often cause small surface displacements and are difficult to detect by the InSAR technique. In addition, the factors affecting the determination of surface displacement due to earthquakes include magnitude and hypocentral depth. In addition, the accuracy of the InSAR method depends on the perpendicular baseline, atmospheric and coherent properties of the master and slave images. In fact, the monitoring of terrain displacement by the InSAR method in densely vegetated and hilly areas such as Kon Tum will have some limitations. To reduce the influence of

atmospheric conditions on the InSAR technique, we propose to detect the impacts of earthquakes in Kon Tum, Vietnam by the PSInSAR method using multi-temporal Sentinel-1A images. The observation period is from March, 2021 to July, 2022.

2. STUDY AREA AND MATERIALS

2.1. Study area

The study area is Kon Plong district, where low-to-moderate earthquakes occurred, and the effects on surrounding areas in Kon Tum province, Vietnam. The boundary and location of Kon Plong district and Kon Tum province are shown in Figures 1a and 1b.

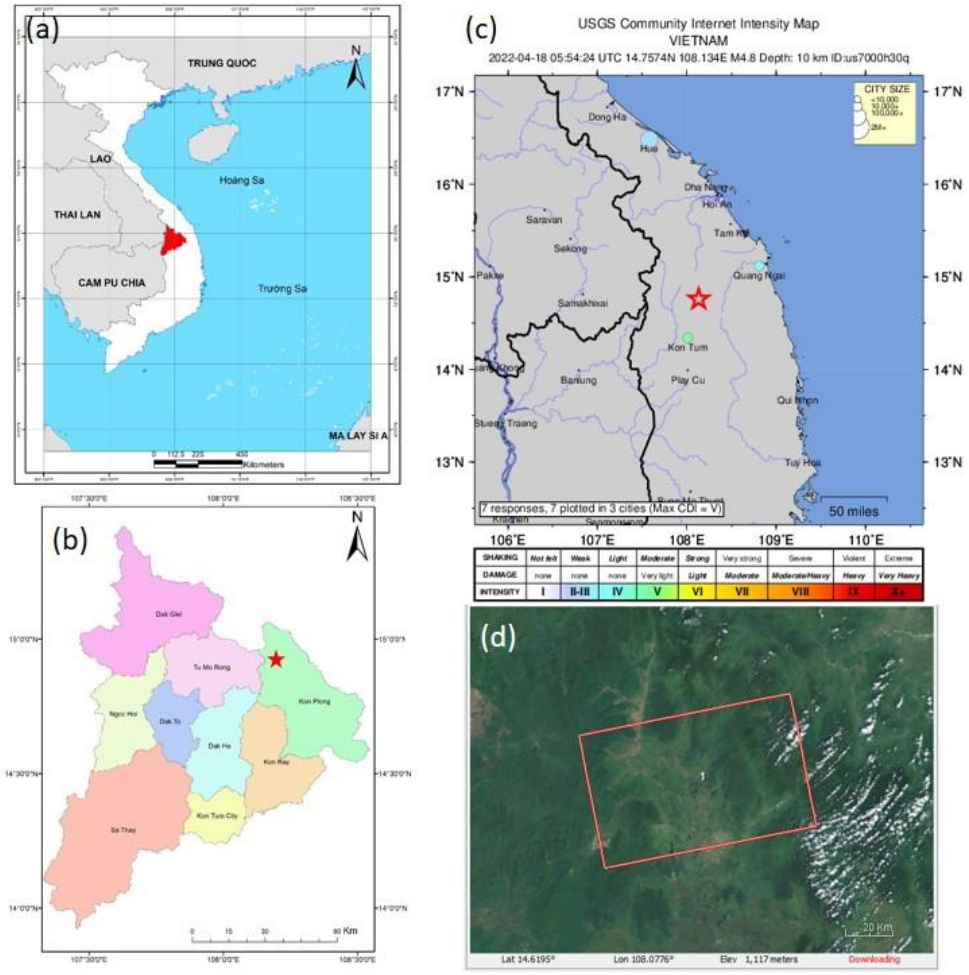

Figure 1. (a) Location Kon Tum in Vietnam; (b) The district of Kon Tum; (c) The Earthquake in Kon Tum are recorded by USGS in 18/04/2022 with 4.8 Richter; (d) The position of Sentinel-1A in the study area

Kon Tum is a province in the north of the Central Highlands, Vietnam. Location coordinates range from 13055'10" to 15027'15" north latitude and from 107020'15" to 108032'30" east longitude. Most of the area is located in the western part of the Truong Son mountains (Annamite Range). The topography is complicated, including mounds, hills, mountains, plateaus, and alternating lowlands. Hills and mountain areas cover two-fifths of the province's area, with an average elevation of 500 m to 700 m. The north has an altitude of 800m to 1200m. The mountains are distributed in the north-northwest direction, running to the east of Kon Tum province. Kon Tum's climate has two distinct seasons: the rainy season (from April to November) and the dry season (from December to March of the next year). There is a difference in temperature between the high mountains in the Northeast with cool weather and the lowland areas in the Southwest with dry and hot weather.

Kon Plong is a mountainous district that is located in the northeast of Kon Tum province. The coordinates of location 14042'N and 108015'E. The topography is hilly, with the Kon Plong plateau occupying the main area of the district. The area has many small rivers and streams. The climate is divided into many sub-regions, including a cold, rainy climate. Kon Plong is a district with a forest coverage of 78% of the natural land area, the highest in Vietnam. Small rice fields are often located next to streams and at the foot of the piedmont slope. The area has no major industrial trees.

The Kon Tum province currently has 28 hydropower plants in operation and 36 hydropower projects under construction. Most of the hydropower plants in Kon Tum are small and medium ones. But it is possible that earthquakes in the area are caused by the buildup of hydroelectric power.

2.2. Materials

Sentinel-1A imagery from the Kon Tum area of Vietnam was used for the experiment. The characteristics of the data are shown in Table 1.

Table 1. The characteristics of Sentinel-1A data

	Sentinel – 1A
Acquisition time	40 scences (18/03/2021 – 11/07/2022)
Data product	Interferometric Wide (IW) - SLC
Polarization	VV - polarization
Imaging frequency	C-band (5.46 Hz)
Bit depth	16 bit

SNAP toolbox software is used to do preprocessing steps on Sentinel-1A data. These steps include applying orbit, back geocoding, processing TOP SAR data, co-registering and repairing data for StaMPS (Stanford Method for Persistent Scatterers) software. In the study, we used an SRTM Digital Elevation Model (DEM) of 90m resolution for removing the topographical content. The steps for calculating PS points are performed by StaMPS software. The experience data consists of 39 Sentinel-1A images. The study area is at location IW1 and burst from 5 to 7 (Figure 1d). Using the SNAP toolbox software, we identified the master image on October 20, 2021, and the other images as slave images. The length of the perpendicular baseline of interference images is shown in Figure 2. Besides, Figure 3 shows the location of the epicenter, the magnitude, and the hypocentral depth of the earthquakes that occurred in Kon Tum from March 2021 to July 2022.

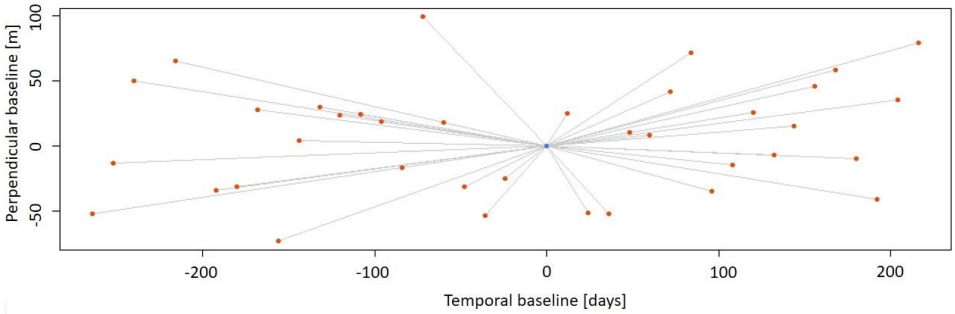

Figure 2: The perpendicular baseline of interference images with the master image on October 20, 2021

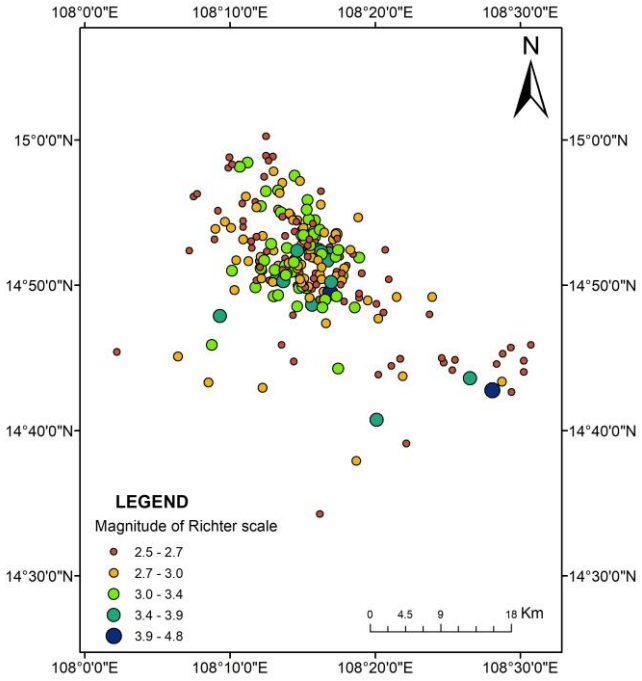

Figure 3. The location of the epicenter earthquakes in Kon Tum province, Vietnam (03/2021 – 07/2022)

3. METHODOLOGY

3.1. Differential Interferometric Synthetic Aperture Radar (DInSAR)

The InSAR technique is applied to estimate the interferometer from two SAR images. At the moment, InSAR is mostly used to detect and monitor surface changes that happen between radar sensor passes in the same scene. In such a case, assuming a surface change occurs during the two SAR acquisition times in the scene, an additional term in the interferometer phase relates to the RADAR line of sight (LOS) component of the surface displacement. By the geometric relationship described in Figure 3, we have (Pepe and Calo, 2017):

$$\Delta\varphi = -\frac{4\pi}{\lambda}\cdot\frac{B_n}{r sin\theta}z + \frac{4\pi}{\lambda}d_{LOS} \tag{1}$$

Where d_{LOS} denotes the projection of the observed deformation in the sensor LOS direction; B_n is the perpendicular baseline; θ are the satellite side-looking angle; z is the surface height.
In order to estimate the interferometric phase term associated with the displacement, the interferometric phase contribution related to the underlying topography must be eliminated from Eq.(1). Specifically, Differential interferometry (DInSAR) consists primarily of the synthesis of a simulated topographic phase screen using a Digital Elevation Model (DEM) of the area and the subtraction, pixel-by-pixel, of these synthetic fringes, leaving just the displacement element. In addition to the deformation component, computed differential SAR interferograms also contain (unwanted) phase components resulting from inadequacies in the knowledge of the real topographic pattern and orbital parameters. Particularly, the variation of the interferometric phase can be described in a more general form as follows (Pepe and Calo, 2017):

$$\Delta\varphi = \Delta\varphi_{displ} + \Delta\varphi_{topo} + \Delta\varphi_{orb} + \Delta\varphi_{atm} + \Delta\varphi_{scatt} + \Delta\varphi_{noise} \tag{2}$$

Where:
$\Delta\varphi_{displ} = \frac{4\pi}{\lambda}d_{LOS}$ provides for the possibility of scatterer displacement on the ground between observations.
$\Delta\varphi_{topo} = -\frac{4\pi}{\lambda}\cdot\frac{B_n}{r sin\theta}\Delta z$ indicates the residual-topography-induced phase resulting from an inaccurate understanding of the real height profile (i.e., the DEM errors Δz).
$\Delta\varphi_{orb}$ provides for residual fringes caused by the use of imprecise orbital data in the topographic phase synthesis;
$\Delta\varphi_{atm}$ indicates the phase components induced by the difference in propagation conditions between the two images (caused by the change in atmosphere and ionospheric dielectric constant);
$\Delta\varphi_{scatt}$ represents the phase components caused by changes in scattering behavior;
$\Delta\varphi_{noise}$contains all phase noise contribution.

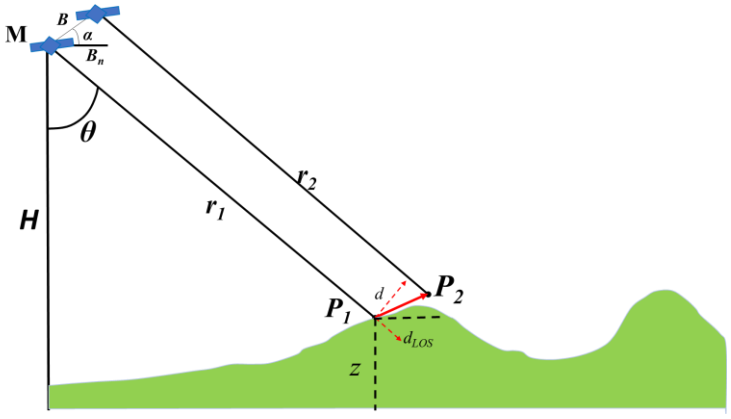

Figure 4. InSAR geometry for the estimation of the displacement of the Earth's surface

In addition, the occurrence of phase unwrapping errors, resulting from an incorrect estimate of 2π-multiple integers to be added to the (measured) InSAR phase to recover the complete (unrestricted) phase, is a further cause of misinterpretation regarding the (wanted) deformation signal.

3.2. Persistent Scatterer Interferometry (PSInSAR)

The purpose of every DInSAR approach is to extract $\Delta\varphi_{displ}$ from $\Delta\varphi$. This necessitates the separation of $\Delta\varphi_{displ}$ from the other phase components of Eq (2). An essential condition for achieving this separation is to analyze pixels

characterized by small $\Delta\varphi_{noise}$, which are often associated with two types of reflectors: those where the radar response is dominated by a powerful reflecting object and is constant over time (Permanent Scatterer, PS) and those where the radar response is constant over time, but is caused by a variety of small scattering objects (Distributed Scatterers, DS) (Crosetto, et al., 2015). PSInSAR is a type of DInSAR techniques that use multiple SAR images recorded over the same area and proper data processing and analysis procedures to distinguish $\Delta\varphi_{displ}$ from the other phase components indicated by Eq (2). The primary results of a PSI study are the deformation time series and the deformation velocity computed over the analyzed PSs or DSs (Figure 4). An additional result of a PSI analysis is the so-called residual topographic error (RTE), which is the difference between the true height of the scattering phase center of a specific PS and the height of the DEM at this point. The RTE is a critical element for achieving precise PS geocoding (Crosetto, et al., 2015). Figure 5 shows the process of the PSInSAR method using SNAP and StaMPS software (Tran, et al., 2021; Nam, et al., 2020).

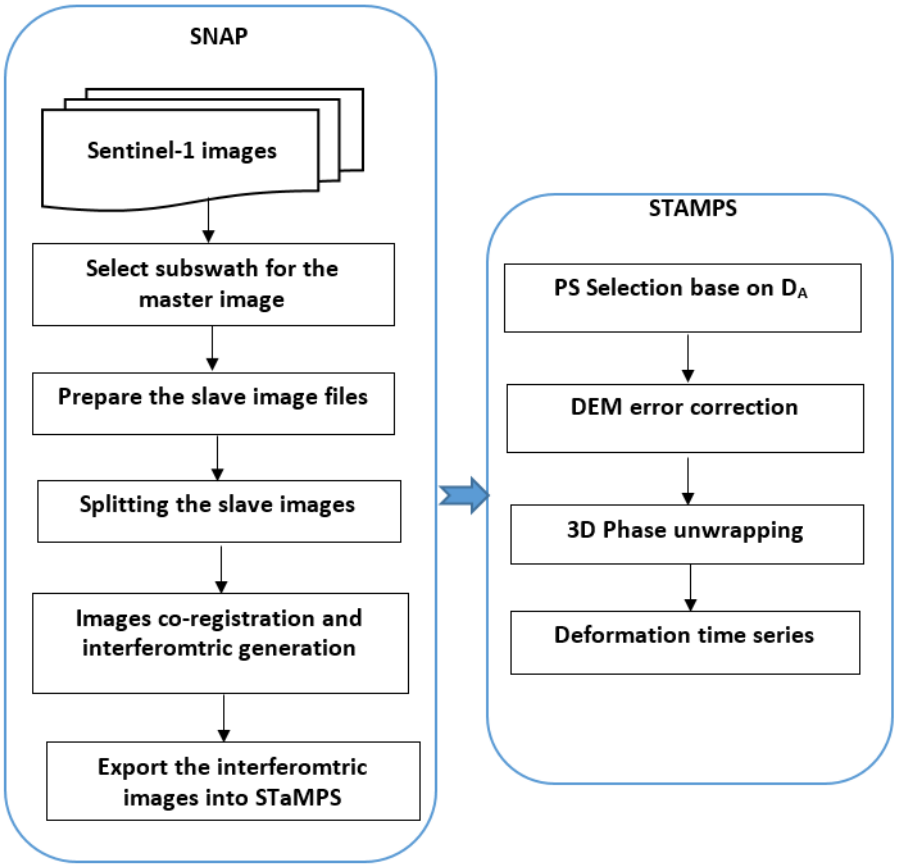

Figure 5. PS-InSAR processing in this research as the flow chart

4. RESULTS AND DISCUSSION

According to the flowchart in Figure 5, we determine the surface displacements of low and moderate magnitude earthquakes in Kon Tum by the DInSAR technique. Table 2 shows the magnitude on the Richter scale and the hypocentral depth of the earthquake in Kon Tum in the acquisition images.

Table 2. The information of the earthquake in Kon Tum province in the acquisition images

Date	Magnitude (Richter)	The hypocentral depth (km)	Date	Magnitude (Richter)	The hypocentral depth (km)
05/05/2021	2.6	16.2	26/09/2021	3; 3.6	15; 8.8
17/05/2021	2.6; 2.5	8.2; 20.1	25/11/2021	2.8	7.9
10/06/2021	2.5	10	12/01/2022	3.7; 3.2	8.2; 8.5
22/06/2021	2.6	8.1	18/04/2022	2.5; 2.9; 2.6; 4.8; 3.6; 3.4; 4.6; 2.5; 4.3	8; 8; 12.1; 10; 8.1; 8.1; 10; 8,2; 10
16/07/2021	2.5; 2.8	8.1; 8.2	17/06/2022	2.6	8.1
02/09/2021	3.0	12	29/06/2022	2.6; 2.7	10; 10

In the days after the earthquake, April 18, 2022, was determined to have had a moderate earthquake with a Richter scale of 4.0-4.8 in the Kon Plong district of Kon Tum province (Figure 1c). Figure 6 depicts the interferogram between the images taken on October 20, 2021 and April 18, 2022 in the study area. Figure 6b shows the interferogram in Kon Tum city. In the study area, the regions with high coherence are mainly urban areas such as Kon Tum city because of the mountainous topography. Hence, InSAR technique conducts in high coherence areas as the urban areas. Based on the interference fringes, we can be seen that the magnitude 4.8 earthquake has an impact on the area that is more than 30 km southwest of the epicenter. Based on the interferogram in Figure 6b, the area has trended the land subsidence.

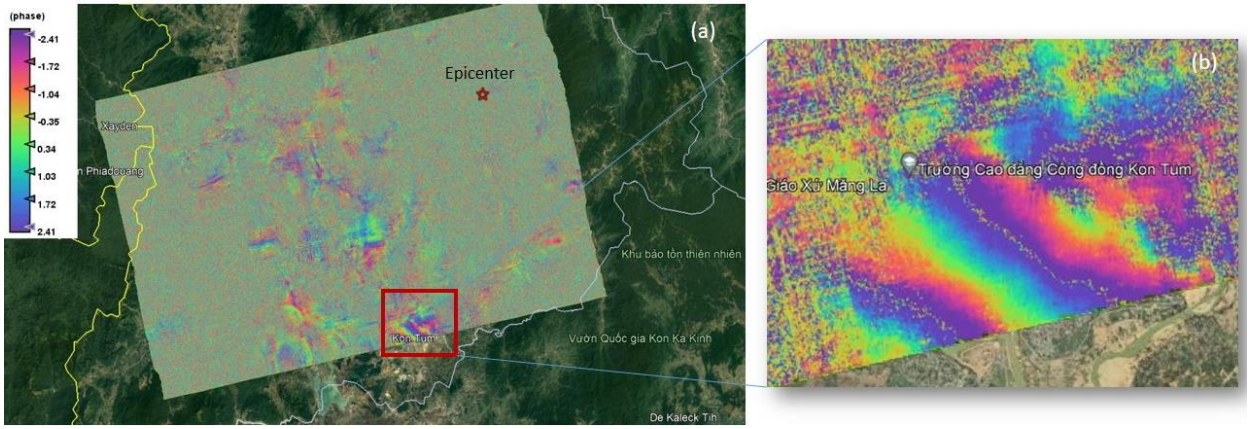

Figure 6. (a) The interferogram by DInSAR method on April 18, 2022; (b) In Kon Tum city

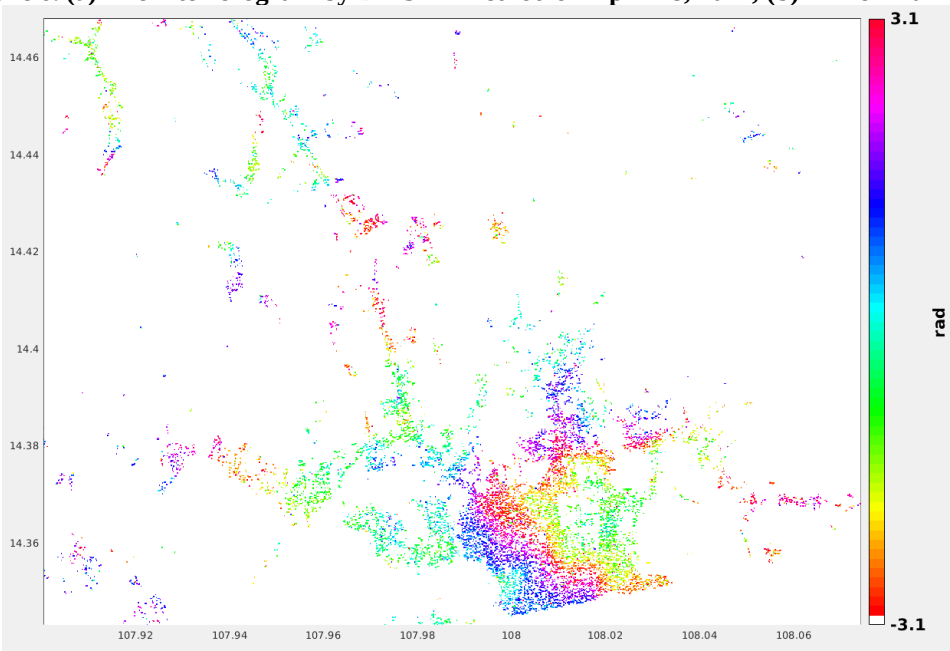

Figure 7. The interferogram of Kon Tum by using PSInSAR method on April 18, 2022

Figure 7 shows similar results when determining phase interference on April 18, 2022 by the PSInSAR method. Using the PSInSAR method, we also determine phase interference at times of low magnitude earthquakes (Figure 8). Figure 8 show that the ground has oscillations at low magnitude earthquakes. The days with great hypocentral depth, such as 20.1 km on May 17, 2021 (Figure 8), clearly have the interferogram.

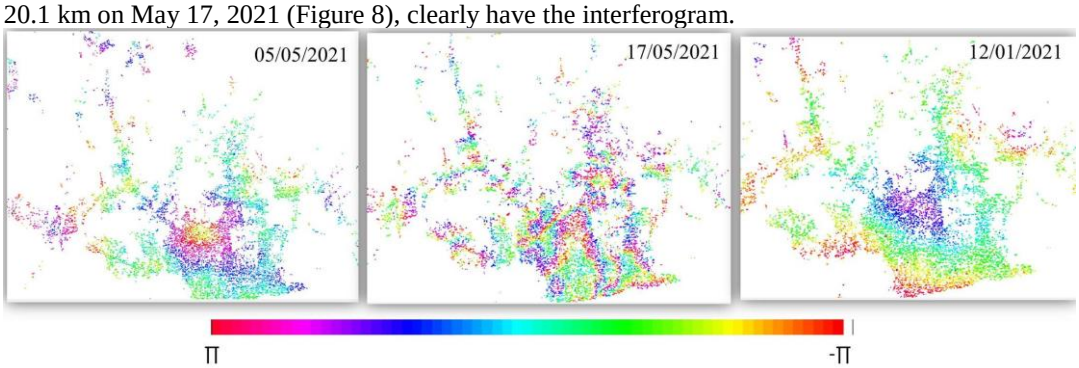

Figure 8. The interferogram of low magnitude earthquake

By using StaMPS software, we determined the mean displacement velocity of the study area (Figure 9). The area has a mean displacement velocity with a range -21.3 mm to +20.3 mm per year. In Figure 10, area A has an upwelling phenomenon, area B has a slumping phenomenon, and Kon Tum city, as area C, tends to be stable. There is no large land subsidence in Kon Tum city.

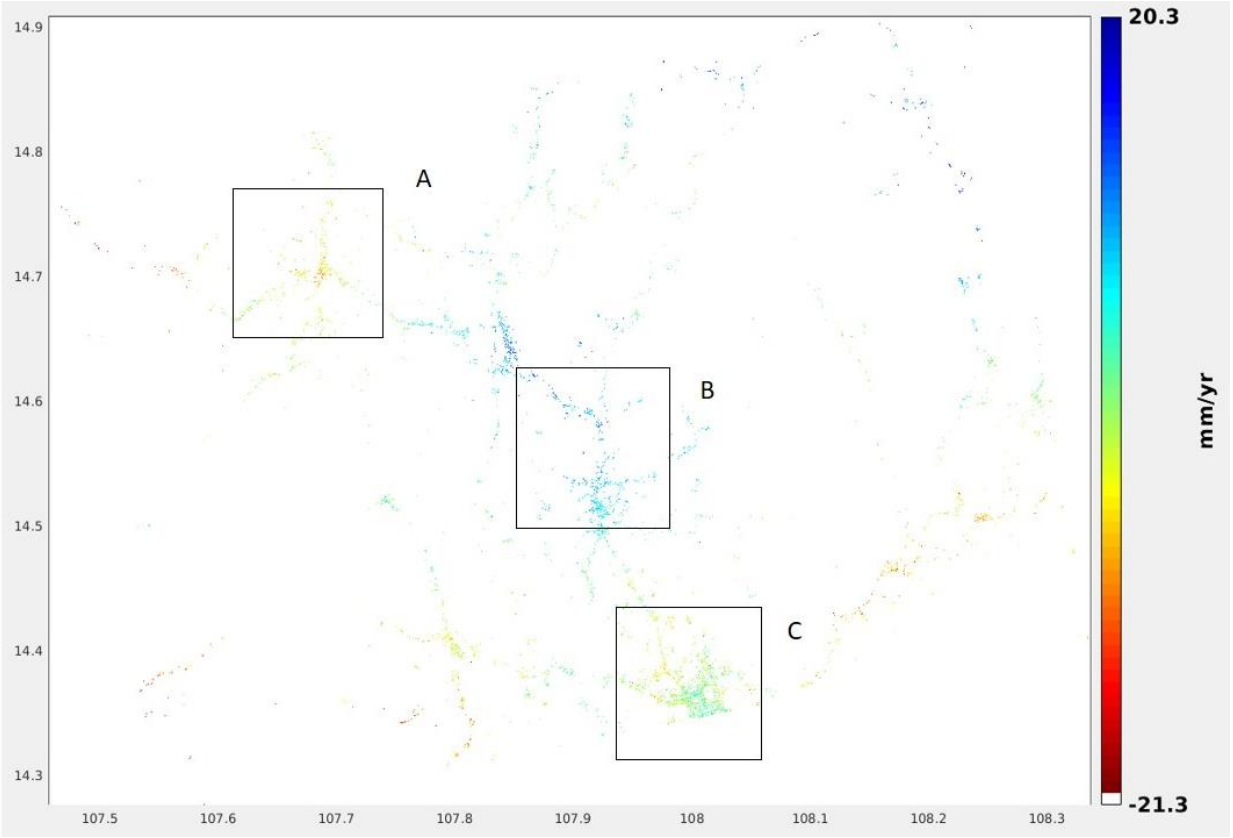

Figure 9. The mean displacement velocity of the study area

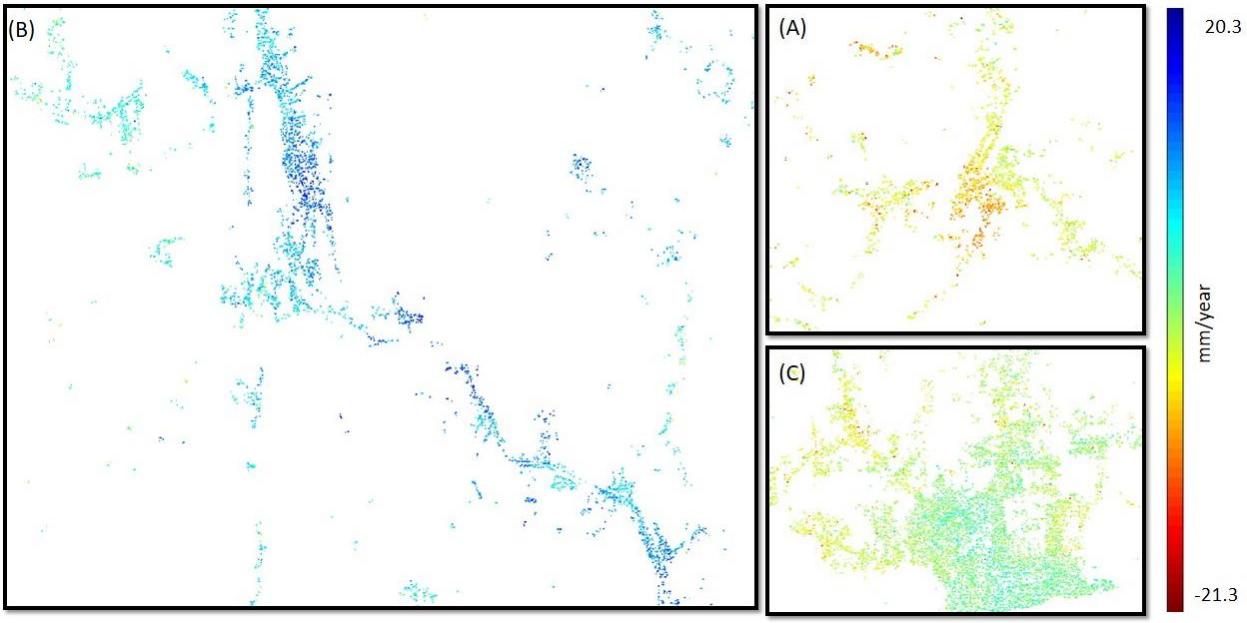

Figure 10. The mean displacement velocity per year of area A, area B, area C

In this article, the author uses StaMPS-Visulizer software (Hooper, et al., 2012) to analyze the surface displacements at PS points in image acquisition time. We analyze surface displacement in three main regions of the study area included in area A, are B and area C of Figure 10.

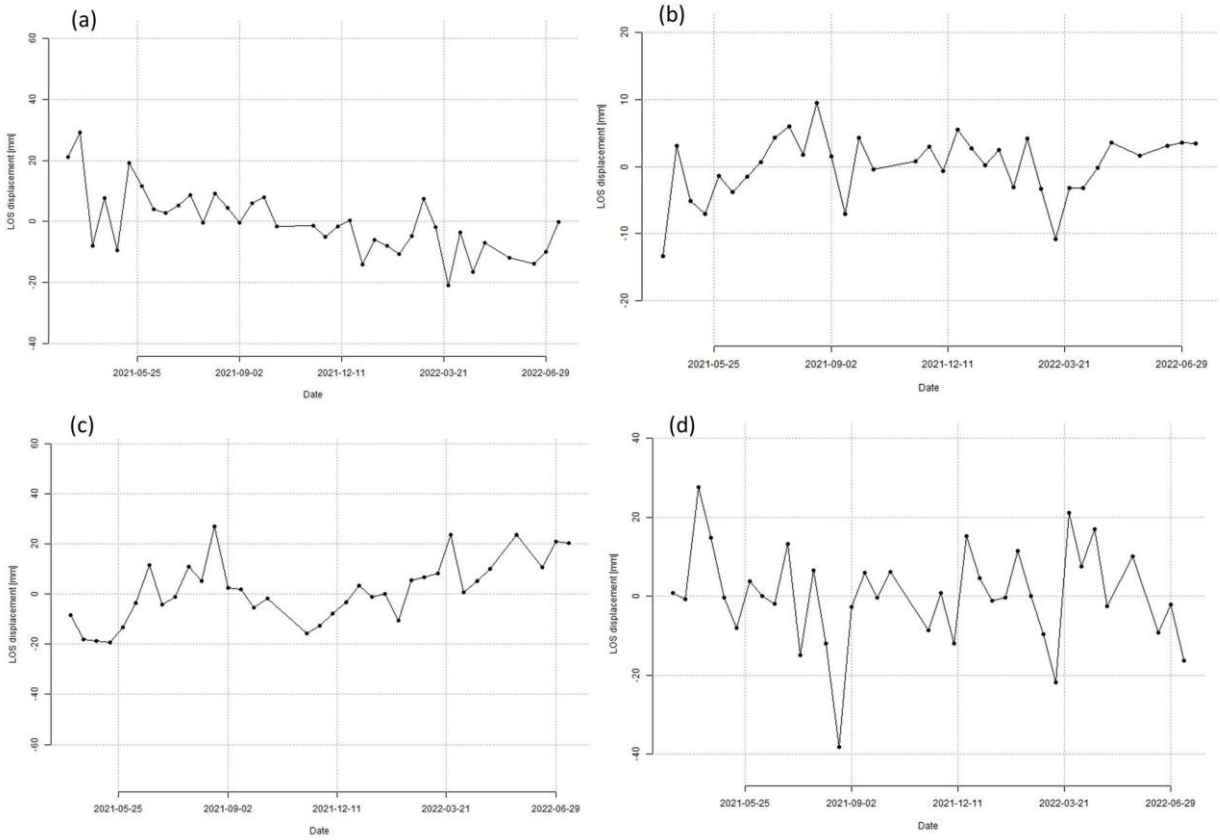

Figure 11. LOS displacement of a PS point; (a) In area A; (b) In area C; (c) In area B; (d) The area nearby the epicenter in Kon Plong district.

The results show that during the period of March 2021 to July 2022, the PS points identified have abnormal land subsidence at the time of the earthquake. There was no subsidence during the study period in area C, which includes the most permanent homes (Figure 11b). There is a fluctuation between -20 mm and +20 mm in Areas A and B, which are primarily composed of dirt road (Figure 11a, 11c). However, there were several unusual changes in the area which is nearby the epicenter (Figure 11d).

5. CONCLUSION

In conclusion, the DInSAR technique is a monitoring tool for low to moderate earthquakes. The results demonstrate that moderate-magnitude earthquakes are typically identifiable on SAR images using the DinSAR technique. PSInSAr, one of the DInSAR methods, permits the estimation of PS points with the use of interferometric time series images. However, the PSInSAR technique can only locate PS points with a high coherence value in urban regions. PS points cannot be identified in areas with dense vegetation, such as the Kon Tum mountain range. Analysis of the mean velocity of displacement in the Kon Tum area shows a range of -21.3 mm to +23.3 mm. At the time of the aftershock, the analysis of multi-temporal interference data at PS points indicates abnormal land subsidence. Evaluation of the capability of the DInSAR technique to detect the impacts of earthquakes in mountainous regions of Vietnam required many studies on different types of data, at different times, and field-level validation. This article's results will also help Vietnam in applying InSAR technology to monitor surface displacement, particularly the effects of earthquakes.

REFERENCES

Bignami, C., Antonioli, A., Atzori, S., Kiratzi, A., Polcari, M., 2020. Mapping InSAR deformation of low and moderate earthquakes. Procedia Computer Science, 180, pp. 214–219.

Catry, T., Villeneuve, N., Froger, J-U., Maggio, G., 2015. InSAR monitoring using RADARSAT-2 data at Piton de la Fournaise (La Reunion) and Karthala (Grande Comore) volcanoes. Geological Society, 426, pp. 505-532.

Crosetto, M., Monserrat, O., Cuevas-González, M., Devanthéry, N., Crippa, B., 2015. Persistent Scatterer Interferometry: A review. ISPRS Journal of Photogrammetry and Remote Sensing, 115, pp. 78-89.

Elske, Z. D., Pedersen, R., Hooper, A., Freysteinn, S., 2012. Subsidence of Askja caldera 2000–2009: Modelling of deformation processes at an extensional plate boundary, constrained by time series InSAR analysis. Journal of Volcanology and Geothermal Research, 213-214, pp.72-82.

Furuya, M. and Satyabala, S.P., 2008. Slow earthquake in Afghanistan detected by InSAR. Geophysical Research Letters, 35, pp. 1-4.

Gatsios, T., Cigna, F., Tapete, D., Sakkas, V., Pavlou, K., Parcharidis, I., 2020. Copernicus Sentinel-1 MT-InSAR, GNSS and Seismic Monitoring of Deformation Patterns and Trends at the Methana Volcano, Greece. Applied Sciences, 10, 6445, pp. 1-23.

Ghayournajarkar, N. and Fukushima, Y., 2020. Determination of the dipping direction of a blind reverse fault from InSAR: case study on the 2017 Sefid Sang earthquake, northeastern Iran, Earth, Planets and Space, 72:64, pp. 1-15.

Ghayournajarkar, N. and Fukushima, Y., 2022. Using InSAR for evaluating the accuracy of locations and focal mechanism solutions of local earthquake catalogues, Geophysical Journal International, 230, pp. 607-622.

Gong, W., Meyer, F., Webley. P. W., Lu, Z., (2011) Methods of InSAR atmosphere correction for volcano activity monitoring, IEEE International Geoscience and Remote Sensing Symposium, pp. 1654-1657.

Hooper, A., Bekaert, D., Spaans, K., Arıkan, M., 2012. Recent advances in SAR interferometry time series analysis for measuring crustal deformation. Tectonophysics, 514-517, pp. 1-13.

Huang, Y., Yu, M., Xu, Q., Sawada, K., Moriguchi, S., Yashima, A., Liu, C., Xue, L., 2014. InSAR-derived digital elevation models for terrain change analysis of earthquake-triggered flow-like landslides based on ALOS/PALSAR imagery. Environmental Earth Sciences, 73 (11), pp. 7661-7668.

Li, Y., Jiang, W., Zhang, J., Li, B., Yan, R., Wang, X., 2021a. Sentinel-1 SAR-Based coseismic deformation monitoring service for rapid geodetic imaging of global earthquakes. Natural Hazards Research, 1, pp. 11-19.

Li, Y., Li, Y., Hu, X., Liu, H., 2021b. Fault Geometry and Mechanism of the Mw 5.7 Nakchu Earthquake in Tibet Inferred from InSAR Observations and Stress Measurements. Remote Sensing, 13, 5142, pp. 1-15.

Liu, J., Hu, J., Li, Z., Ma, Z., Shi, J., Xu, W., Sun, Q., 2022. Three-Dimensional Surface Displacements of the 8 January 2022 Mw6.7 Menyuan Earthquake, China from Sentinel-1 and ALOS-2 SAR Observations. Remote Sensing, 14, 1404, pp. 1-14.

Moro, M., Saroli, M., Stramondo, S., Bignami, C., Albano, M., Falcucci, E., Gori, S., Doglioni, C., Polcari, M., Tallini, M., Macerola, L., Novali, F., Costantini, M., Malvarosa, F., Wegmuller, U., 2017. New insights into earthquake precursors from InSAR. Scientific reports, 7, 12035, pp. 1-11.

Nam, B.X., Tran, V. A., Bui, L. K., Long, N.Q., Le, T.T.H., Goyal, R., (2021). Mining-Induced Land Subsidence Detection by Persistent Scatterer InSAR and Sentinel-1: Application to Phugiao Quarries, Vietnam. Proceedings of the International Conference on Innovations for Sustainable and Responsible Mining, Springer, 108, pp. 18-38.

Pepe, A. and Calo, F., 2017. A Review of Interferometric Synthetic Aperture RADAR (InSAR) Multi-Track Approaches for the Retrieval of Earth's Surface Displacements. Applied Sciences, 7, 1264, pp. 1-39.

Tong, X., Xu, X., Chen, S., 2022. Coseismic Slip Model of the 2021 Maduo Earthquake, China from Sentinel-1 InSAR Observation. Remote Sensing, 14, 436, pp. 1-10.

Tran, V. A., Tran, Q. C., Nguyen, D. A., Ho, T. M. D., Hoang, A. T., Ha, T. K., Bui, D. T., 2021. Subsidence Assessment of Building Blocks in Hanoi Urban Area from 2011 to 2014 Using TerraSAR-X and COSMO-SkyMed Images and PSInSAR. Remote Sensing and GIScience, Springer, Switzerland, pp. 127-150.

Zhao, L., Liang, R., Shi, X., Dai, K., Cheng, J., Cao, J., 2021. Detecting and Analyzing the Displacement of a Small-Magnitude Earthquake Cluster in Rong County, China by the GACOS Based InSAR Technology. Remote Sensing, 13, 4137, pp. 1-10.

Nam, B. X., Anh, T. V., Bui, L. K., Long, N. Q., Thu Ha, T. L., & Goyal, R. (2021). Mining-Induced Land Subsidence Detection by Persistent Scatterer InSAR and Sentinel-1: Application to Phugiao Quarries, Vietnam. In Proceedings of the International Conference on Innovations for Sustainable and Responsible Mining , Springer, Cham, pp. 18-38

Pepe, A. and Calo, F., 2017. A Review of Interferometric Synthetic Aperture RADAR (InSAR) Multi-Track Approaches for the Retrieval of Earth's Surface Displacements. Applied Sciences, 7, 1264, pp. 1-39.

Tong, X., Xu, X., Chen, S., 2022. Coseismic Slip Model of the 2021 Maduo Earthquake, China from Sentinel-1 InSAR Observation. Remote Sensing, 14, 436, pp. 1-10.

Tran, V. A., Truong, X. Q., Nguyen, D. A., Longoni, L., & Yordanov, V. 2021. Landslides Monitoring with Time Series of SENTINEL-1 Imagery in Yen Bai Province-Vietnam. International Society for Photogrammetry and Remote Sensing, 4, 46, pp.197-203

Zhao, L., Liang, R., Shi, X., Dai, K., Cheng, J., Cao, J., 2021. Detecting and Analyzing the Displacement of a Small-Magnitude Earthquake Cluster in Rong County, China by the GACOS Based InSAR Technology. Remote Sensing, 13, 4137, pp. 1-10.